Studies into the Detection of Buried Objects (Particularly Optical Fibres) in Saturated Sediment. Part 5: An Acousto-Optic Detection System

R.C.P. Evans and T.G. Leighton

ISVR Technical Report No 313

April 2007

SCIENTIFIC PUBLICATIONS BY THE ISVR

Technical Reports are published to promote timely dissemination of research results by ISVR personnel. This medium permits more detailed presentation than is usually acceptable for scientific journals. Responsibility for both the content and any opinions expressed rests entirely with the author(s).

Technical Memoranda are produced to enable the early or preliminary release of information by ISVR personnel where such release is deemed to the appropriate. Information contained in these memoranda may be incomplete, or form part of a continuing programme; this should be borne in mind when using or quoting from these documents.

Contract Reports are produced to record the results of scientific work carried out for sponsors, under contract. The ISVR treats these reports as confidential to sponsors and does not make them available for general circulation. Individual sponsors may, however, authorize subsequent release of the material.

Studies into the detection of buried objects (particularly optical fibres) in saturated sediment. Part 5: An acousto-optic detection system

R C P Evans and T G Leighton

ISVR Technical Report No. 313

April 2007

UNIVERSITY OF SOUTHAMPTON

INSTITUTE OF SOUND AND VIBRATION RESEARCH

FLUID DYNAMICS AND ACOUSTICS GROUP

Studies into the detection of buried objects (particularly optical fibres) in saturated sediment. Part 5: An acousto-optic detection system

by

R C P Evans and T G Leighton

ISVR Technical Report No. 313

April 2007

Authorized for issue by
Professor R J Astley, Group Chairman

ACKNOWLEDGEMENTS

CONTENTS

FIGURE CAPTIONS

ABSTRACT

This report is the last in a series of five, designed to investigate the detection of targets buried in saturated sediment, primarily through acoustical or acoustics-related methods. Although steel targets are included for comparison, the major interest is in targets (polyethylene cylinders and optical fibres) which have a poor acoustic impedance mismatch with the host sediment. Whilst previous report in this series have considered techniques for the detection of difficult targets in general when they are buried in saturated sediment, this particular report discusses one specific type of target: the optic fibre. The underlying theory, and a laboratory test, are investigated in order to assess the feasibility of its practical use.

The use of optic fibres as distributed sensors is discussed, the most notable example of such a system being the OTDR. Non-linear optical processes that could be exploited in a distributed sensor are also discussed. The Brillouin effect is given special consideration, and it is noted that the associated Brillouin frequency shift depends on variations in temperature and, of particular interest, variations in strain.

The related, acousto-optic effect, is also investigated, and it is shown that both length and refractive index changes (in response to an applied strain) can cause a change in the optical phase within a fibre. Moreover, pressure sensitivity is shown to be related to the elastic properties of the fibre jacket material. A greatly enhanced sensitivity is predicted if the cladding has a high compressibility (which is expected to be the case for non-metallised fibre optic cables).

An experiment is performed to investigate whether a conventional OTDR could be used to detect acoustically-generated stresses within an optic fibre. A change in the back-scattered power in the optical window of the detector is found to occur. These results are discussed in terms of the practicality of a working system.

This series of reports is written in support of the article "The detection by sonar of difficult targets (including centimetre-scale plastic objects and optical fibres) buried in saturated sediment" by T G Leighton and R C P Evans, written for a Special Issue of *Applied Acoustics* which contains articles on the topic of the detection of objects buried in marine sediment. Further support material can be found at http://www.isvr.soton.ac.uk/FDAG/uaua/target_in_sand.HTM.

LIST OF SYMBOLS

a   An adjustment variable

b   An adjustment variable

c   An adjustment variable

c_g Speed of light in a glass fibre

e   Exponential constant (2.71828182)

E_Y Young's modulus

$E_Y^{(i)}$ Young's modulus of a layer in a multilayer cylinder (where the use of (i) defines the layer of interest in a multilayer cylinder, such that i=0 corresponds to the core)

F   Net axial force

f_0 Carrier frequency of light beam

f_k Acoustic frequency in kilohertz

i   An index related to the layers in an optic fibre, where $i = 0$ denotes the core, and $i = n$ denotes the nth layer

$\mathbf{k_a}$ Wave vector of an acoustic wave

K_b Bulk modulus

$\mathbf{k_B}$ Wave vector of a Brillouin signal

$\mathbf{k_p}$ Wave vector of an optical pump signal

l   Length

LPR   Landau-Placzek ratio

m   A positive integer variable

n   A non-zero positive integer denoting the number of layers in the

	multilayer cylinder which represents a given optical fibre
NA	Numerical aperture
n_c	Refractive index of the cladding of an optic fibre
n_f	Refractive index of the core of an optic fibre
n_r	Refractive index
Δn_r	Change in refractive index when a material is deformed
p_0	Pressure acting on the outer surface of the fibre
Δp_0	Pressure change occurring within an optical fibre
p_{EM}	Average elasto-optic coefficient
p_{EM11}	{1,1} element of the elasto-optic coefficient tensor
p_{EM12}	{1,2} element of the elasto-optic coefficient tensor
r	Radial distance
$r^{(0)}$	Radius of inner interface of multilayer cylinder
$r^{(1)}$	Radius of middle interface of multilayer cylinder
$r^{(2)}$	Radius of outer interface of multilayer cylinder
S	The fraction of recaptured optical power at the source
t	Time
T_{abs}	Absolute temperature
T_f	Fictive temperature
$u^{(i)}$	Radial displacement
$U_0^{(i)}, U_1^{(i)}$	Lamé solution parameters (where the use of (i) defines the layer of interest in a multilayer cylinder, such that i=0 corresponds to the core)
v_a	Acoustic velocity in a glass fibre
v_g	Group velocity of a light pulse
W_i	Optical power launched into an optic fibre
W_0	The value for $W_0^{(i)}$ which is constant for all layers in a multilayer cylinder

$W_0^{(i)}$	Lamé solution parameter (where the use of (i) defines the layer of interest in a multilayer cylinder, such that i=0 corresponds to the core)
W_{dB}	Relative optical back-scatter
$w^{(i)}$	Axial displacement
W_R	Rayleigh back-scattered optical power
z	The axial position relative to the end of an optic fibre
Δz_{min}	spatial resolution for propagation of light pulse down optic fibre
α_B	Brillouin scattering coefficient
α_R	Rayleigh back-scattering coefficient
α_t	Total attenuation coefficient
β_T	Isothermal compressibility at the fictive temperature, T_f
ε_r, $\varepsilon_r^{(i)}$	Radial strains in an optic fibre core layer (where the use of (i) defines the layer of interest in a multilayer cylinder, such that i=0 corresponds to the core)
ε_z, $\varepsilon_z^{(i)}$	Axial strains in an optic fibre core layer (where the use of (i) defines the layer of interest in a multilayer cylinder, such that i=0 corresponds to the core)
ε_θ, $\varepsilon_\theta^{(i)}$	Torsional strains in an optic fibre core layer (where the use of (i) defines the layer of interest in a multilayer cylinder, such that i=0 corresponds to the core)
ϕ_{rad}	Phase delay
ϕ_{rad}	Phase shift due to pressure change in optic fibre
κ	Boltzmann's constant (1.380×10^{-23} J K^{-1})
λ	Wavelength
$\lambda^{(i)}$	Lamé parameter for layer (i) of a multilayer cylinder (where i=0

	corresponds to the core)
λ_p	Free space wavelength of an optical pump source
λ_r	Wavelength of refractive index variations
$\mu^{(i)}$	Lamé parameter for layer (i) of a multilayer cylinder (where i=0 corresponds to the core)
ν	Poisson's ratio
$\nu_Y^{(i)}$	Poisson's ratio for a layer in a multilayer cylinder (where the use of (i) defines the layer of interest in a multilayer cylinder, such that i=0 corresponds to the core)
π	Pi (≈ 3.141592654)
θ_s	Scattering angle
ρ_g	Density of a glass fibre
σ_r, $\sigma_r^{(i)}$	Radial stresses in an optic fibre core layer (where the use of (i) defines the layer of interest in a multilayer cylinder, such that i=0 corresponds to the core)
σ_z, $\sigma_z^{(i)}$	Axial stresses in an optic fibre core layer (where the use of (i) defines the layer of interest in a multilayer cylinder, such that i=0 corresponds to the core)
σ_θ, $\sigma_\theta^{(i)}$	Torsional stresses in an optic fibre core layer(where the use of (i) defines the layer of interest in a multilayer cylinder, such that i=0 corresponds to the core)
τ_w	Pulse width
ω_a	Acoustic wave frequency
ω_B	Brillouin frequency

ω_p	Pump frequency
ω_S	Brillouin frequency shift

∇	Differential operator $\left(\dfrac{\partial}{\partial x}, \dfrac{\partial}{\partial y}, \dfrac{\partial}{\partial z} \right)$

1   Introduction

This report is the last in a series of five, designed to investigate the detection of targets buried in saturated sediment, primarily through acoustical or acoustics-related methods. Although steel targets are included for comparison, the major interest is in targets (polyethylene cylinders and optical fibres) which have a poor acoustic impedance mismatch with the host sediment. The first report outlined the problem, introducing the technology of cable design and deployment, detection and recovery[1]. The second described the test tank apparatus, including the bistatic acoustic sensors and the positioning system[2], and the third provided results for acoustic penetration of a rough sediment, outlining relevant theories to describe the process[3]. The fourth report tested a variety of signal processing systems for their abilities to detect objects buried in the saturated sediment, using a bistatic acoustic system[4]. Thus far, the investigation has focused on the general detection of objects buried in the seabed. However, it has been useful to concentrate on one particular class of object, that being fibre optic telecommunication cables. This also reflects the interests of Cable & Wireless, the sponsors of this research. As introduced in the first report in this series[1], there may be an alternative, novel means of detecting this type of object. This possibility is investigated in the current report.

An alternative to the acoustic detection approach is to find some way of actively changing the properties of a buried cable to facilitate its detection by some other means. This can be achieved using an external acoustic field, which can affect the optical transmission properties of the fibres within the cable. This field could be

---

[1]   T G Leighton and R C P Evans, Studies into the detection of buried objects (particularly optical fibres) in saturated sediment. Part 1: Introduction. *ISVR Technical Report No.* 309 (2007).

[2]   T G Leighton and R C P Evans, Studies into the detection of buried objects (particularly optical fibres) in saturated sediment. Part 2: Design and commissioning of test tank. *ISVR Technical Report No.* 310 (2007).

[3]   R C P Evans and T G Leighton, Studies into the detection of buried objects (particularly optical fibres) in saturated sediment. Part 3: Experimental investigation of acoustic penetration of saturated sediment. *ISVR Technical Report No.* 311 (2007).

[4]   R C P Evans and T G Leighton, Studies into the detection of buried objects (particularly optical fibres) in saturated sediment. Part 4: Experimental investigations into the acoustic detection of objects buried in saturated sediment. *ISVR Technical Report No.* 312 (2007).

projected as a beam from an acoustic source mounted on a remotely operated vehicle (ROV) or a surface vessel. Subsequently, it should be possible to determine the position of the cable by using established optical techniques to detect when the footprint of the acoustic beam passes over it.

The detection protocol associated with this technique is summarised in figure 1. Three cables are shown in the example. If the requirement is for cable B to be found, then the acousto-optic detection system should be connected to its input. The position of the cable is determined using the fact that it will be directly beneath the footprint of the acoustic beam at the time at which a change in the optical transmission properties of the fibres is detected. An advantage of this system is that even if the beam passes over cables A and C there can be no danger of confusing them with the broken cable, since the detection system is connected directly to cable B.
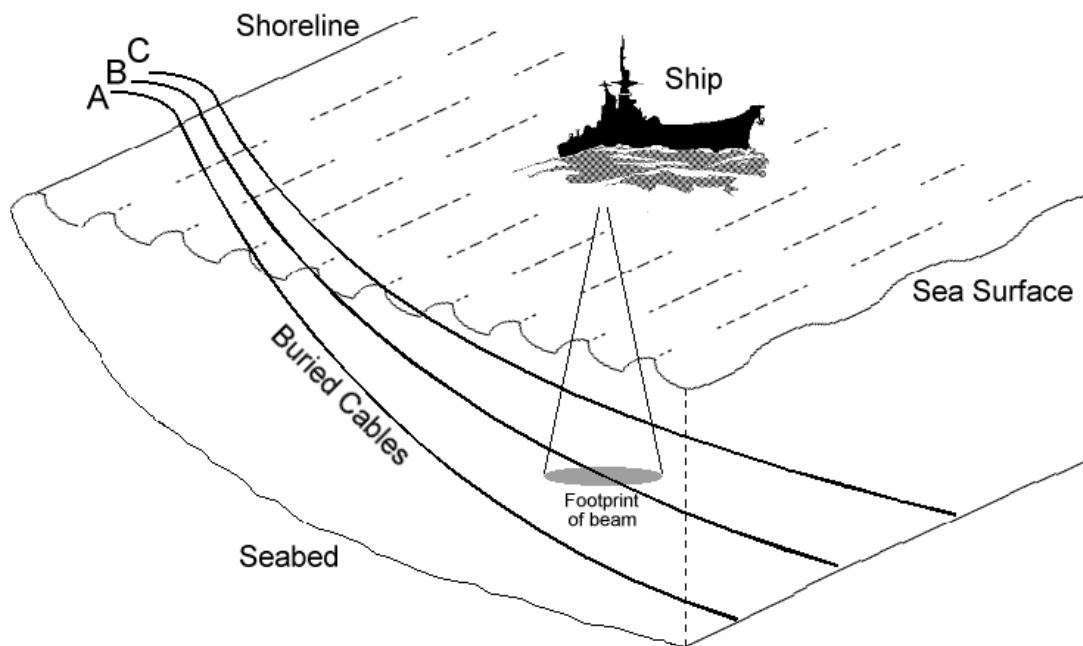
Figure 1 *The detection protocol associated with an acousto-optic detection system. In this scenario, an acoustic beam is projected from a surface vessel (though it could also be projected from an ROV). As the footprint of the beam passes over cable B, its affect on the optical transmission properties of the inner fibres may be detected using a land-based system. By comparing the position of the footprint over time with the time of detection, it should be possible to determine the location of the cable.*

It should be noted that it is not the cable that is being detected using this approach. Instead the influence of the acoustic source is detected by the fibre within the cable, which acts as a sensor. The advantage of this method is that the issues surrounding scattering at the water-sediment interface, and back-scattering from the target, become largely irrelevant. Simply, by directing an acoustic beam of sufficiently high acoustic intensity at the seabed, it should be possible to locate the target. The issues related to determining the required intensity are the subject of the remainder of this report.

The concept of distributed fibre optic sensors, including the optical time domain-reflectometer (OTDR), are introduced in section 2. Non-linear optical processes, which are of particular interest in this investigation, are discussed in section 3. Of the different non-linear processes that are considered, the Brillouin effect is identified as being the most useful. Brillouin OTDR systems are discussed in section 4.

Another important mechanism, which is related to Brillouin scattering, is the acousto-optic effect. This is exploited in optic fibre hydrophone systems, as noted in section 5. The pressure sensitivity of jacketed optic fibres is calculated, and the implications for the acousto-optic detection of submarine telecommunication cables is discussed.

Following this theoretical study, an experiment involving an OTDR system is presented (see section 6). It was decided to investigate whether a conventional OTDR could be applied directly to the cable detection problem. The requirements of this study were significantly different from the research activities detailed in previous reports in this series[1-4]. Therefore, the assistance of the project's sponsors, Cable & Wireless, was called upon to provide the necessary optical test and measurement equipment.

2   Distributed Fibre Optic Sensors

A change in the propagation characteristics of an optic fibre due to some external influence (*i.e.*, sound) can be detected by measuring the modulation of light passing through it [1, 2]. A 'distributed' fibre optic sensor enables the external influence to be spatially resolved along the length of the fibre as a continuous function of distance.

This may be achieved by taking advantage of the known, finite, propagation time of light in the fibre. The detection length is limited only by the intrinsic fibre loss.

A distinct advantage of the fibre sensor over other sensing technology is that it requires no local power. Energy exchanged during the interaction comes from the acoustic source and the propagating light beam. It is also mechanically rugged and offers a high sensitivity with low self-noise. However, the need for repeaters in submarine cables could be a major drawback in the context of this study (see section 2.2 of the first report in this series[1]), since the acoustic modulation of the optical signal would be lost during the conversion into an electrical signal. Fortunately, unrepeatered systems based on the erbium-doped fibre amplifier (EDFA) should not pose the same problem since they do not need to convert optical signals into electrical signals for amplification.

In order to measure the modulated light beam it is necessary to gain access to one end of the fibre. In this investigation it is assumed that access will only be available at the same end as the optical source. Therefore, it is necessary to identify a light scattering mechanism that can be used to carry some fraction of the modulated light back to the source [3].

2.1 Scattering in Optic Fibres

As light passes through a medium it generates an oscillating dipole moment at each molecule it encounters. These radiate, or scatter, electromagnetic (EM) energy in every direction. If the medium is perfectly homogeneous, the vector sum of the scattered fields in any direction, other than in the forward direction, is zero. However, if the medium contains fluctuations in the dielectric constant, light will be scattered in other directions. Static fluctuations scatter light elastically, *i.e.*, there is no frequency shift between the incident and scattered light. In contrast, dynamic fluctuations give rise to inelastic scattering that results in frequency shifted components [4].

An optic fibre is, essentially, a one-dimensional propagating medium. For the purpose of observing scattered light, only the forward and backward directions have any

significance. Light scattered in any direction other than within the fibre capture angle[5] will be lost, resulting in a transmission loss along the fibre. Light scattered in the backward direction, provided it is within the capture angle of the fibre, will be scattered towards the source.

Elastic scattering is the dominant loss mechanism in optic fibres at the low attenuation window at a wavelength of around 1 550 nm. There are also a number of important inelastic scattering mechanisms in optic fibres, including Raman and Brillouin scattering. These are considered in more detail in section 3.

2.2   Back-Scatter Sensors

The significant source of elastic scattering in optic fibres is Rayleigh scattering[6], caused by random inhomogeneities in the refractive index which are of a small scale compared with the wavelength of incident light. These inhomogeneities are caused by thermal density and compositional variations which are 'frozen' into the glass on cooling during its manufacture. The Rayleigh back-scattering coefficient is given by

$$\alpha_R = \frac{8\pi^3}{3\lambda^4} n_r^8 p_{EM}^2 \kappa T_f \left[\beta_T - \left(\rho_g v_a^2 \right)^{-1} \right] \tag{1}$$

where λ is the optical wavelength, n_r is the refractive index, p_{EM} is the average elasto-optic coefficient, κ is Boltzmann's constant, T_f is the 'fictive temperature', β_T is the isothermal compressibility at T_f, ρ_g is the density of the glass, and v_a is the acoustic velocity in the material.

The Rayleigh back-scattering coefficient is proportional to λ^{-4} which implies that there is a considerable reduction in fibre attenuation as the operating wavelength is

---

[5] The fibre capture angle is quantified in terms of the numerical aperture, NA, and is a measure of the light-gathering power of the system [5]. For an optic fibre,

$$NA = \sqrt{\left(n_f^2 - n_c^2 \right)} \tag{F 1}$$

where n_f and n_c are, respectively, the refractive indices of the fibre core and the surrounding cladding.

[6] In this series of reports, Rayleigh scattering is first introduced in the context of electromagnetic wave scattering in the first report in this series (see footnote 1), and is referred to again in the context of acoustic scattering in section 3 of the fourth report in this series (see footnote 4).

increased. It is also highly sensitive to the refractive index and is proportional to the temperature at which the fluctuations are frozen into the glass.

For fused silica glass: $T_f = 1\ 400$ K; $\beta_T = 6.9 \times 10^{-11}$ Pa^{-1}; $n = 1.46$; $p_{EM} = 0.286$; $\rho_g = 2\ 200$ kg m^{-3}; and $v_a = 5\ 800$ m s^{-1}. Therefore, at a wavelength of $\lambda = 1\ 550$ nm, $\alpha_R \approx 100 \times 10^{-6}$ m^{-1}.

2.3   Optical Time-Domain Reflectometry

The back-scattering optic fibre sensor is best exemplified by the forerunner of all distributed fibre optic sensors, the optical time-domain reflectometer (OTDR). In 1985 it was considered feasible to use the OTDR for fault location over a length of fibre of up to 100 km, corresponding to an attenuation in optical power of around 30 dB at 0.2 dB km^{-1} [6, 7]. Modern OTDRs offer remarkably high precision over lengths that exceed this early prediction.
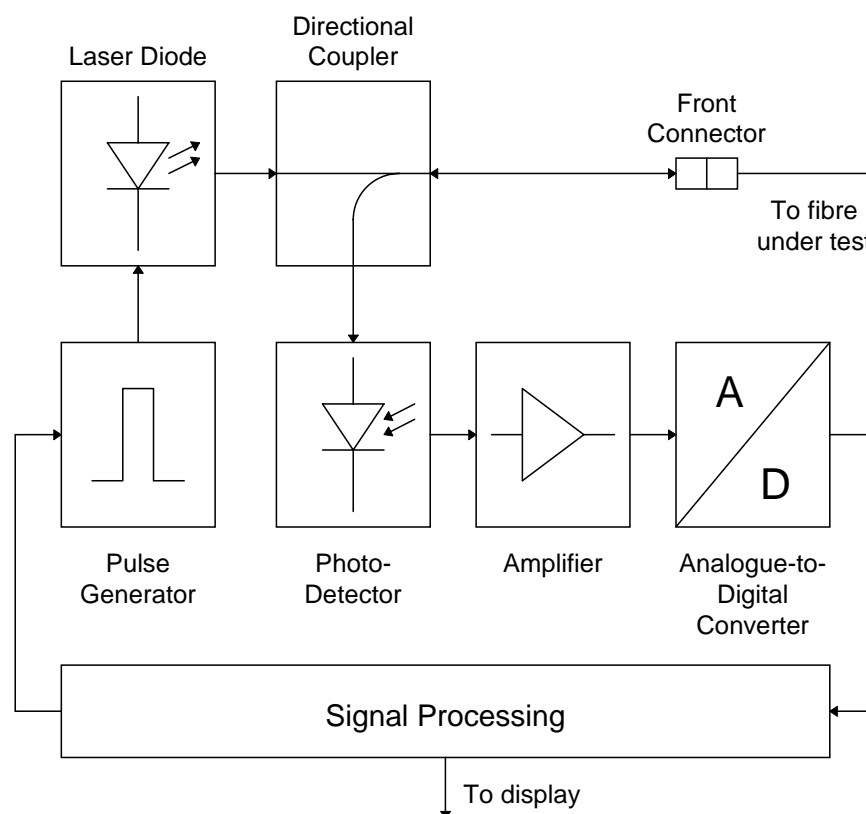
Figure 2 *The architecture of an optical time-domain reflectometry system.*

In operation the OTDR launches a short pulse of laser light into a fibre under test. As the pulse propagates through the fibre, loss occurs due to Rayleigh scattering from random, microscopic variations in the refractive index of the fibre core. A fraction of the light is scattered back towards the detector. The processing electronics measures the level of back-scattered light as a function of time relative to the input pulse. If the fibre is homogeneous and subject to a uniform environment, the intensity of the back-scattered light decays exponentially with time because of the intrinsic loss in the fibre. Back-scattered power detected at the input end as a function of time is given by

$$W_R(t) = \frac{1}{2} W_i \alpha_R S \tau_w \exp(-\alpha_t v_g t) \tag{2}$$

where W_i is the optical power launched into the fibre, S is the fraction of recaptured optical power, α_R is the Rayleigh back-scattering coefficient, τ_w is the pulse width, v_g is the group velocity of the light pulse, and α_t is the total attenuation coefficient [8]. The time taken for the optical pulse to travel to, and then to return from, a scatter at a distance, z, from the input end of the fibre is represented by the parameter, t (*i.e.*, $z = v_g t / 2$).
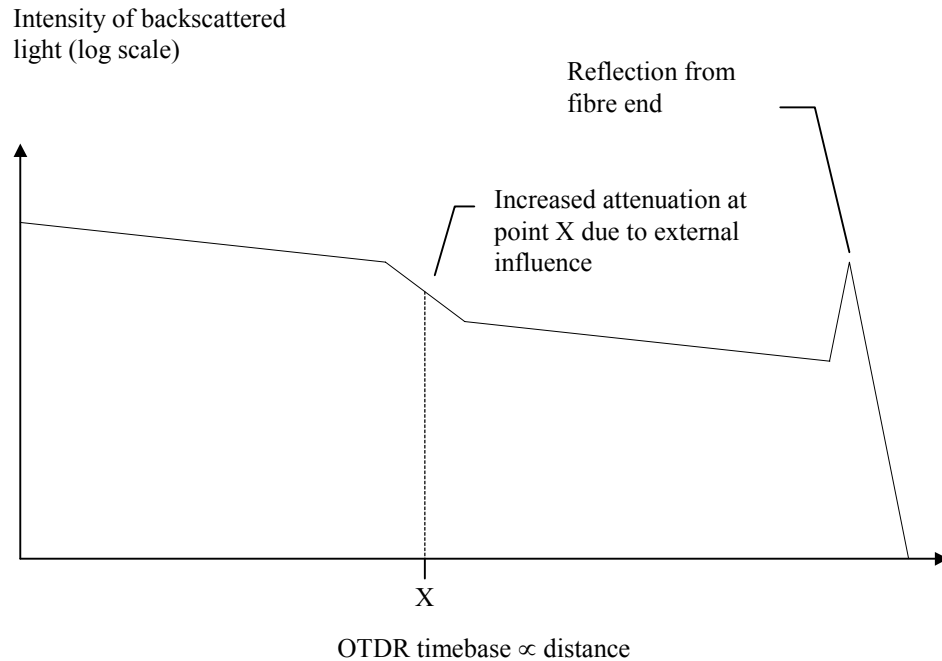
Figure 3 The OTDR output trace. The intensity of the back-scattered signal is displayed as a function of time (proportional to fibre length). An almost constant attenuation is observed over the length of the fibre except at point X where some external influence has caused the attenuation to increase.

The exponential term represents the fibre attenuation characteristics. It is assumed that the loss experienced by the back-scattered signal and the forward pulse are equal. Hence, the slope of the logarithm of this detected signal is equal to the loss coefficient at location z:

$$\frac{d(\ln W_R)}{dz} = -2\alpha_t \tag{3}$$

Regions of high loss are indicated by an increase in the slope of the OTDR trace, as shown in figure 3. Spatial resolution is determined by the input pulse width:

$$\Delta z_{min} = \frac{v_g \tau_w}{2} \tag{4}$$

However, the low energy associated with short pulses results in a restricted range [9].

In short, the OTDR is a fibre optic sensor that inherently measures attenuation as a function of distance. It has proven itself to be an invaluable diagnostic tool in the telecommunication industry, being used for the detection of fibre damage and measurement of fibre performance.

2.4 Practical Considerations

For long-distance, high-bandwidth communications, monomode fibres are preferred to the multimode type, despite having a core diameter of just 5 μm compared with a more manageable 50 - 60 μm for multimode fibres [9]. However, they have the attraction that there is no differential mode dispersion[7] so the available bandwidth can be very high.

---

[7] Differential mode dispersion results from the different paths, or modes of propagation, available to light in multimode fibre. For a single wavelength of light and a uniform refractive index, every ray travels at the same speed but arrives at different times. This effect is mitigated by using 'graded index fibre', where the core is made of concentric layers of glass of varying refractive index. Rays propagating further from the axis of the fibre, and so travelling a longer path, spend most of their journey in glass of a lower refractive index than rays propagating closer to the axis. Therefore, rays which travel a longer distance also travel faster and arrive at roughly the same time as those that travel a shorter distance.

The maximum resolution of an OTDR system is limited by chromatic dispersion[8] which depends on the linewidth of the source. A dispersion of just a few ns km^{-1} generates an error in the distance measurement of some tens of metres for a 100 km length of cable. (Chromatic dispersion is a major problem for extremely long-distance (> 1 000 km), high-bandwidth cables [4]. Current research in the use of soliton pulses that maintain their shape as they propagate through the medium, and wavelength division multiplexing that makes optimum use of available bandwidth, is seeking to overcome this limitation.)

Contaminating elements in glass, introduced during the manufacturing process, absorb energy from incident light. The amount of energy absorbed depends on the proportion of impurity atoms present. Absorption produced by transition metals is strongly dependent on frequency and can be avoided by choosing a suitable wavelength for the light source. The other main absorption mechanism is due to the presence of the hydroxyl ion, OH^-, which has a pronounced absorption peak at 2 800 nm and the harmonics 1 400 nm, 970 nm and 750 nm. The position of the peaks can be seen clearly in the frequency-attenuation curve shown in figure 4.

The 800 - 900 nm band is popular for low-cost, short-haul systems. A better choice for telecommunication is the 1 300 nm minimum dispersion wavelength. However, most modern long-distance systems use the narrow window around the 1 550 nm minimum absorption wavelength.

OTDR measurements are further complicated by the conditions at the fibre break. Fibre ends which have been snapped or broken cause random dispersion of light, limited only by the numerical aperture. A reflecting, complete break appears as a clear discontinuity in the back-scatter profile and is the easiest fault to detect. Conversely, a non-reflecting, partial break is the most difficult to detect since the change in back-scatter power level may be very small [9].

---

[8] Chromatic, or normal, dispersion occurs because different frequencies of light propagate through a medium at different speeds. In general, at shorter wavelengths the 'phase speed' of light in a medium is less than at longer wavelengths. Therefore, the shorter wavelengths in a pulse of light in an optic fibre will travel more slowly than the longer wavelengths, causing the pulse to spread out in time. The effect is mitigated by using a light source with a narrow spectral linewidth.
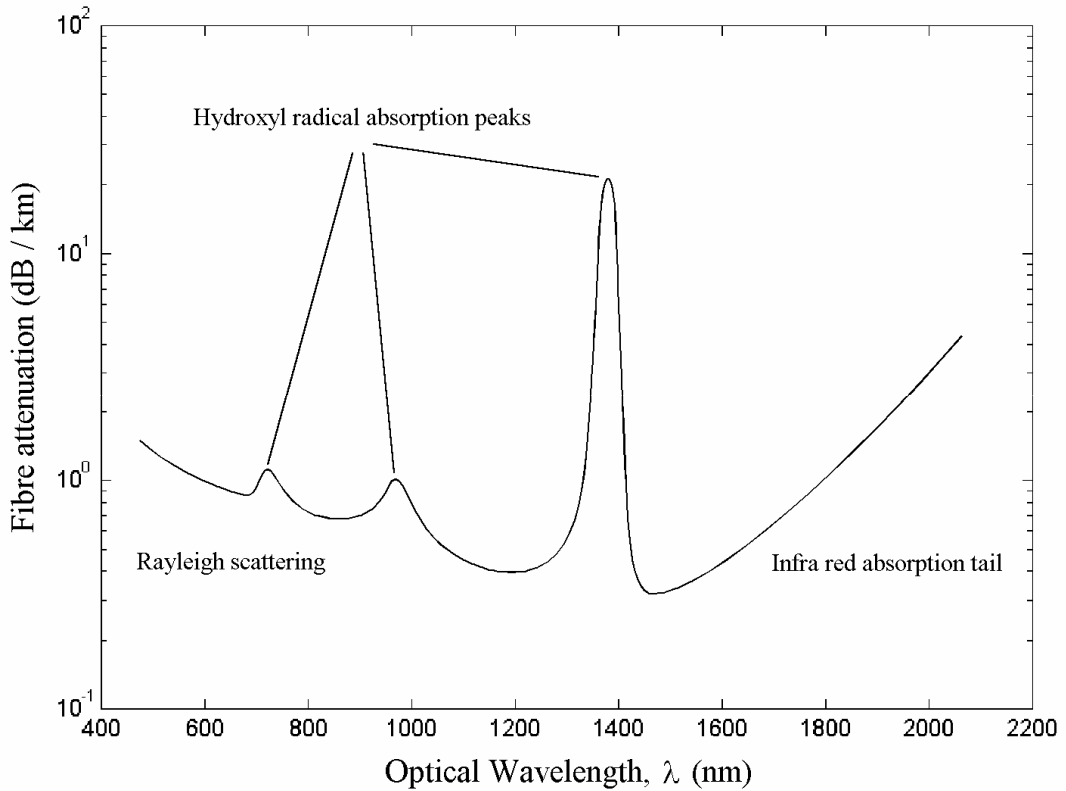
Figure 4 *The characteristic optical attenuation spectrum of glass optic fibres [10].*

Finally, microbending losses can affect the accuracy of an OTDR loss measurement. It is well known that dielectric waveguides lose power by radiation if their axes are curved (as noted in section 3.3 of the first report in this series[1]). Marcuse derived a curvature loss formula for optic fibres by expressing a general solution of Maxwell's equations for the field outside the fibre as a superposition of cylindrical outgoing waves [11, 12].

It is not possible to determine whether the losses measured by an OTDR are caused by absorption or radiation from bends. Submarine telecommunication cable is usually laid in a straight line, only deviating to avoid seafloor hazards, so bending losses do not cause much of a problem. However, this loss mechanism can severely limit the effectiveness of an OTDR in distributed sensing applications. Sensors which make use of non-linear optical effects are able to give much less ambiguous measurements.

3   Non-Linearity in Fibre Transmission

Non-linear processes in monomode, optic fibre transmission systems have been referred to, briefly, in section 2. There are four important processes to consider: Raman scattering; Brillouin scattering; self-phase modulation; and parametric, four-photon mixing [13]. These can lead to signal loss, pulse spreading, crosstalk and even physical damage to the optic fibre.

- **Raman Scattering.** This process occurs under the influence of focused, high-energy laser pulses. The back-scattered signal consists of light of the same frequency and weak, sideband components. The difference between these sidebands and the incident frequency is characteristic of the vibrational modes of molecules in the material [14, 15].

- **Brillouin Scattering.** This results from the interaction between light and thermally generated acoustic waves in the medium. The acoustic wave produces density variations which result in a periodic modulation of the material dielectric constant. Scattered light is, effectively, Doppler-shifted by the movement of the acoustic wave [15, 16]. This process will be detailed in section 3.1.

- **Self-Phase Modulation.** This is a broadening of the signal spectrum at high intensities which, in turn, causes pulse spreading through chromatic dispersion [13]. (In passing, it should be noted that different pulse waveforms, such as soliton pulses [17], can cause intensity dependent pulse narrowing which decreases the net broadening from group-velocity dispersion.)

- **Four-Photon Mixing.** This is a parametric interaction between light of different frequencies which generates new frequencies on either side of the pump frequency [13]. This is not a serious problem in transmission systems because of the need for phase matching in single-mode fibres and high powers in multimode fibres.

The extremely low-loss fibres and high-power, narrow-linewidth lasers used in submarine cable systems make non-linear effects important. In monomode fibres these effects can appear at optical powers of only a few milliwatts. However, fibre non-linearities have enormous potential for distributed sensing applications.

The Raman and Brillouin scattering processes give rise to a difference in frequency between the incident light and the scattered light. Components which lose energy in the scattering process, and therefore have lower frequency, are referred to as Stokes components [18]. Those which gain energy and increase in frequency are referred to as anti-Stokes components [18]. The relative spectral positions of the different scattering mechanisms are illustrated in figure 5.
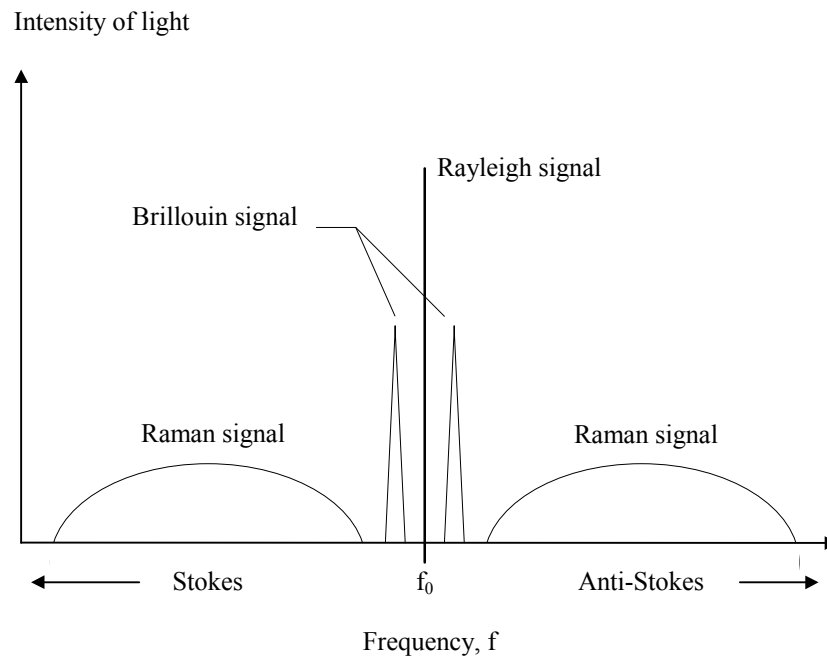
Figure 5 *The positions of Rayleigh, Brillouin and Raman scattered light relative to the incident light beam of frequency,* f_0 *[3]. (Note that these axes are not to scale.)*

The choice of operating wavelength has important consequences for advanced OTDR systems that are based on non-linear interactions. For a 1 550 nm system, the wide bandwidth occupied by the Raman signal means that it occupies the region of strongest absorption in the frequency-attenuation curve. The Brillouin interaction, on the other hand, occupies a much narrower bandwidth and is closer in frequency to the Rayleigh signal. This means that it can make much better use of the minimum dispersion window.

Reflections from fibre ends are also important in advanced OTDR systems. The Brillouin signal peaks at a frequency that is close to that of the optical source. Therefore, a strong reflection makes it hard to detect Brillouin scattering from close to

the end of the fibre. Conversely, the peak of the Raman signal is much further from the source frequency. This means that low loss and low crosstalk separation between the input optical pulse and the back-scattered light pulse can be realised. However, the Raman signal has the disadvantage of a very weak return which is around 30 dB below the Rayleigh signal.

Brillouin scattering has certain advantages over Raman scattering when used for the detection of strain variations over long lengths of optic fibre (*i.e.*, lengths in excess of 100 km). These advantages are noted in section 4. Raman scattering will not be given any further consideration in this series of reports. A physical description of Brillouin scattering is presented in the following section. In section 5, the related acousto-optic effect is also presented, and an experiment is described in section 6 to test the feasibility of using an OTDR to detect acoustically generated stresses in an optic fibre.

3.1   Brillouin Scattering

Brillouin scattering is of particular interest in this application since, not only is the intensity of spontaneous scattering dependent on temperature, but its frequency is dependent on both temperature and strain. Hence, the Brillouin frequency shift is a mechanism for detecting pressure variations generated by a probing acoustic beam.

The modulation of the dielectric constant can cause the incident light beam to be reflected according to Bragg's law. This states that constructive interference takes place if the wavelength of the acoustic modulation, λ_r, is related to the wavelength of the incident light (or 'pump') in the medium, λ_p / n_r, by

$$\lambda_r = \frac{m\lambda_p}{2n_r \sin\left(\frac{\theta_s}{2}\right)} \tag{5}$$

where m is a positive integer which allows for higher order scattering, and θ_s is the angle between the incident and scattered waves, as shown in figure 6. Note that λ_p is the 'free space' wavelength of the pump source.
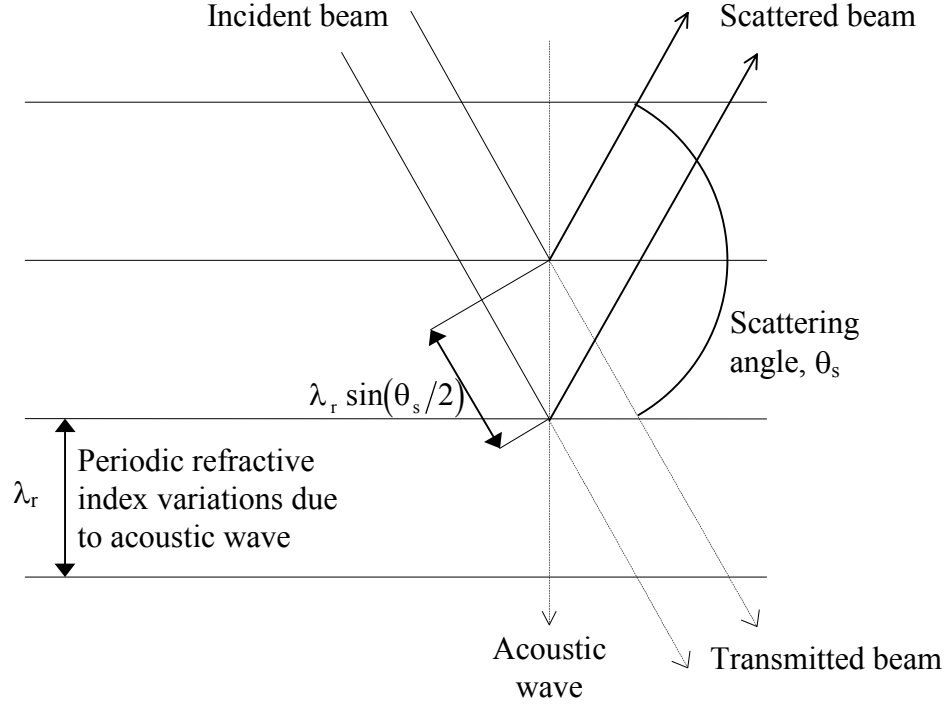
Figure 6 *Bragg scattering from periodic refractive index variations in an otherwise homogeneous medium. The scattered beam will only be coherent if the path length, $2\lambda_r \sin(\theta_s/2)$, is an integer multiple of the wavelength of the incident beam, λ_p/n_r.*

Since both energy and momentum must be conserved during the scattering event, the frequencies and wave vectors of the three waves are related by

$$\omega_B = \omega_p \pm \omega_a \quad \text{and} \quad \mathbf{k_B} = \mathbf{k_p} \pm \mathbf{k_a} \tag{6}$$

where ω_B, ω_p and ω_a are the frequencies of the Brillouin, pump and acoustic waves and $\mathbf{k_B}$, $\mathbf{k_a}$ and $\mathbf{k_p}$ are, respectively, the wave vectors of the Brillouin, pump and acoustic waves in the medium. The sign of the acoustic component is determined by whether it is travelling towards or away from the incident beam.

Bragg's law can be applied if $|\mathbf{k_a}| \approx \dfrac{1}{m}|\mathbf{k_p}|$. Hence,

$$|\mathbf{k_a}| = \frac{2}{m}|\mathbf{k_p}|\sin\left(\frac{\theta_s}{2}\right) \tag{7}$$

Since $\omega_a = |\mathbf{k_a}|v_a$,

$$\omega_a = \frac{2}{m}\left|\mathbf{k_p}\right| v_a \sin\left(\frac{\theta_s}{2}\right) \tag{8}$$

The Brillouin shift, ω_S, is the difference between the frequencies of the incident light and the scattered light. Equation (6) indicates that this equal to the acoustic frequency, ω_a. Given $\left|\mathbf{k_p}\right| = \frac{2\pi n_r}{\lambda_p}$,

$$\omega_S = \pm \frac{4\pi n_r v_a}{m\lambda_p} \sin\left(\frac{\theta_s}{2}\right) \tag{9}$$

In the forward direction ($\theta_s = 0$), the frequency shift is zero. Light scattered in this direction is coincident with, and therefore indistinguishable from, the incident light. Only the back-scattered light ($\theta_s = \pi$), which has a Brillouin frequency shift of $4\pi n_r v_a / \lambda_p$, has any significance.

The Brillouin scattering coefficient, α_B is similar in form to the Rayleigh back-scattering coefficient. However, as the scattering is from thermally generated moving acoustic waves instead of frozen in fluctuations, there is a proportional dependence on temperature, T_{abs}.

$$\alpha_B = \frac{8\pi^3}{3\lambda^4} n_r^8 p_{EM}^2 \kappa T_{abs}\left(\rho_g v_a^2\right)^{-1} \tag{10}$$

The ratio of the Rayleigh to Brillouin scatter is known as the Landau-Placzek ratio, LPR [3]. From equations (1) and (10),

$$LPR = \frac{T_f}{T_{abs}}\left(\beta_T \rho_g v_a^2 - 1\right) \tag{11}$$

At a temperature of 4 °C, and using the values given in section 2.2, LPR is 20.8. Therefore, each of the two Brillouin components (Stokes and anti-Stokes) is approximately 16 dB below the Rayleigh signal.

Above a certain threshold power, the back-scattered light extracts energy from the incident pump beam and so experiences a process of amplification. The effect is then no longer spontaneous but is said to be stimulated Brillouin scattering (SBS). As SBS

grows from what is originally a spontaneous signal, its frequency also has a temperature and strain dependence [3].

4   Brillouin Back-Scatter Systems

The principle of operation of the Brillouin optical fibre sensor is similar to that of the OTDR, the main difference being that the scatter mechanism is Brillouin instead of Rayleigh. Hence the term 'Brillouin OTDR' (BOTDR) is used [19].

There are two important practical differences: a narrow linewidth source must be used so that the Rayleigh back-scatter does not mask the Brillouin signal; and the Brillouin back-scatter must be separated from the Rayleigh back-scatter at the detector using some form of filter. For a distributed temperature sensor, all that is required is to analyse the intensity of the back-scattered Brillouin signal as a function of time. If both the intensity and frequency of the back-scattered light are analysed it is possible to implement a combined distributed temperature and strain sensor.

It should be noted that Raman OTDRs are also in common use. However, the Brillouin effect offers a number of advantages over the Raman effect for distributed sensing [3]:

- The back-scatter intensity is an order of magnitude higher than that of Raman and, therefore, provides the possibility of greater range.

- Owing to the small frequency shift between the incident and back-scattered light, maximum advantage may be taken of the low attenuation window at 1 550 nm.

- The Brillouin signal may be recovered by optically heterodyning the back-scattered signal with a reference signal, resulting in a more convenient frequency for signal processing.

The disadvantages associated with Brillouin back-scatter sensors are a reduced sensitivity to temperature and difficulty in separating the Brillouin and Rayleigh signals due to their small frequency separation.

The dependency of the Brillouin shift on variations in temperature and strain are summarised in the following sections. The strain dependence is of particular interest

in this study, since acoustic waves incident on an optic fibre should give rise to a variation in strain. The temperature dependence is presented for completeness.

4.1   Temperature Dependence of the Brillouin Shift

The refractive index and the velocity of acoustic waves both vary as a function of temperature. The two effects are additive, but the contribution by the acoustic velocity variation is, by far, the dominant one. The velocity of acoustic waves in the fibre is given by

$$v_a = \sqrt{\frac{E_Y(1-v)}{(1+v)(1-2v)\rho_g}} \tag{12}$$

where E_Y is Young's modulus, v is Poisson's ratio and ρ_g is the density of the glass [20]. Young's modulus and density vary as a function of temperature. However, the temperature coefficient of volume expansion is very small (around $2.5 \times 10^{-6} / \,^{\circ}C$ [21]) so density can be assumed to remain constant. In the range 0 - 200 °C the optical frequency variation is approximately 1 MHz / °C.

4.2   Strain Dependence of the Brillouin Shift

When a material is deformed, *e.g.*, by an acoustic wave, there is a change in refractive index, Δn_r, which is related to the applied axial strain, ε_z, by

$$\Delta n_r = -\frac{n_r^3}{2}\left[\varepsilon_z v p_{EM11} - \varepsilon_z(1-v)p_{EM12}\right] \tag{13}$$

where p_{EM11} and p_{EM12} are the {1,1} and {1,2} elements respectively of the elasto-optic coefficient tensor[9] [22]. (Axial (ε_z) and radial (ε_r) strains are related through Poisson's ratio by, $v = -\varepsilon_r / \varepsilon_z$ [23]).

---

[9]   When a material is formed, its optical properties change due to strain S_{kl}. This is known as the elasto-optic or acoustic-optic effect. The latter name is given because, in practice, the strain is usually produced by a propagating acoustic wave, often at ultrasonic frequencies.

$$\Delta \eta_{ij} = p_{ijkl} S_{kl} \tag{f.1}$$

Since Poisson's ratio, ν, and Young's modulus, E_Y, are also dependent on strain, the variation of acoustic velocity must also be considered [24]. The effects of refractive index and acoustic velocity are usually in opposition, but the acoustic velocity variation is dominant. By substituting equations (12) and (13) into equation (9), the formula for the Brillouin frequency shift, an expression for the frequency-strain sensitivity of an optic fibre can be deduced [3].

The radial sensitivity of a typical glass fibre is around $9\ \text{kHz}/\mu\text{strain}$. This corresponds to an applied stress, or pressure, sensitivity of approximately $130\ \text{Hz}/\text{kPa}$ (given that the Young's modulus of glass is around $7 \times 10^{10}\ \text{Pa}$ [25]). Even with a sensitive interferometric system this modulation would be very hard to detect, given that the optical frequencies are in the terahertz band.

The related acousto-optic effect is investigated in the following section. It will be seen that the pressure sensitivity equation includes a term that is similar to equation (14). However, the acousto-optic effect also takes into account the physical change in the length of the fibre, which may result in a much higher sensitivity.

5   Optic Fibre Hydrophones

A variety of optic fibre hydrophone systems, that take advantage of the acousto-optic effect, have been developed in recent years [26]. The most successful are those based on interferometry [27]. In such systems the change in relative phase between a light beam injected into a fibre and the same beam exiting the fibre is measured. This phase change is caused by changes in physical length and refractive index which are directly

---

where p_{ijkl} is the elasto-optic coefficient tensor. Noting that $\Delta\eta_{ij}$ and S_{kl} are both rank 2 symmetric tensors, we can rewrite (f.1) in abbreviated subscript notation as

$$\Delta\eta_I = p_{IJ}\,S_J \tag{f.2}$$

$$\Delta\eta_I = \Delta\eta_{ij}, \qquad p_{IJ} = p_{ijkl} \tag{f.3}$$

The variable p_{IJ} represents the elasto-optic (or acoustic-optic) coefficient matrix.

related to changes in pressure. The advantage of using an interferometric system is that a very high sensitivity can be achieved[10].

The total phase change is the sum of many small changes which are accumulated as the incident light is transmitted. However, in this application, access is only available to one end of the fibre. Therefore, to measure the change in phase, light must be returned from the far end. This is possible if the break in the fibre is reflective; light will be returned along the same path, experiencing twice the phase change. However, in the case of a non-reflecting, partial break, it may not be possible to implement this kind of sensor [9].

The phase delay of an optical signal propagating at speed, c_g, in a fibre of length, l, is $\phi_{rad} = \omega l / c_g$. Hence, the pressure sensitivity of the optical phase in a fibre can be defined as $\Delta\phi_{rad} / \phi_{rad} \Delta p_0$, where $\Delta\phi_{rad}$ is the shift in phase due to a pressure change, Δp_0. If this pressure change results in a fibre core axial strain, ε_z, and a radial strain, ε_r, it has been shown that [29]

$$\frac{\Delta\phi_{rad}}{\phi_{rad}} = \varepsilon_z - \frac{n_r^2}{2}\left[\varepsilon_r\left(p_{EM11} + p_{EM12}\right) + \varepsilon_z p_{EM12}\right] \tag{14}$$

The first term represents the physical length change in the fibre. The second term is similar to equation 14, and represents the refractive index modulation of the core. These are frequently in opposition, but the physical length change is usually the more important effect.

Practical optic fibres comprise a glass core surrounded by layers, which are also made of glass, with an outer jacket of plastic. In a telecommunication cable several fibres are bundled together to form a single fibre unit which is, itself, sheathed in layers of insulation, armour, *etc*. (see section 2.1 of the first report in this series[1]). However, an understanding of the physical processes at work can be obtained from a model of a

---

[10] An example of the sensitivity that can be achieved with an interferomteric system is the measurement of the SI unit of length. The metre is defined as being 1 650 763.73 wavelengths of a particular line in the spectrum of krypton in a vacuum. The measurement required to set up this standard involves forming an interference pattern between two mirrors, and counting the number of fringes which cross the field of view as one mirror is moved relative to the other. The movement of $^1/_{10}$ of a fringe can just be detected, so the accuracy attainable is about 1 part in 10^7 [28].

single, multi-layered fibre. Hughes and Jarzynski derived a complete three-dimensional model of the strains in such a fibre [20, 30].

These researchers have also shown that a much simpler 'plane-strain' model, which requires significantly less computation, can be used. This was found to be in good agreement with the three-dimensional model (within 1.5 % for a typical three layer fibre), with the accuracy reducing as the number of layers was increased. A mathematical description of the plane-strain model and its relationship to the pressure sensitivity (equation (14)) is presented in Appendix A.

The elastic and elasto-optic coefficients are not generally known for the variety of glasses used for optic fibres. Previous studies of the sensitivity of high silica content fibres have assumed that they were equal to those of fused silica [31]. In this study, however, data was made available by Cable & Wireless for a typical monomode fibre. Parameters for the core and three layers are presented in table 1.

Fibre Parameter	Core	Layer 1	Layer 2	Layer 3
Composition	SiO_2	SiO_2 (95 %)	S_iO_2	Silicone
	GeO_2 (trace)	B_2O_3 (5 %)		
Radius (µm)	2	13	42	125
Young's modulus (GPa)	72	65	72	0.0035
Poisson's ratio	0.17	0.149	0.17	0.49947
p_{EM11}	0.126	-	-	-
p_{EM12}	0.27	-	-	-
Refractive index	1.458	-	-	-

Table 1 *The composition, dimensions and elastic and elasto-optic coefficients of a typical single mode optic fibre.*
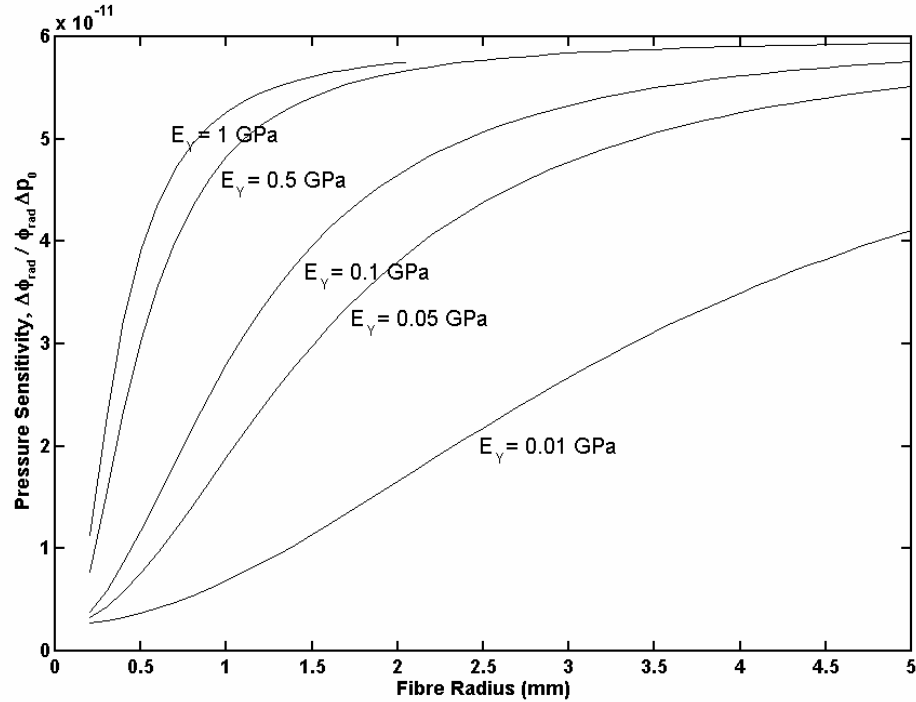
Figure 7 *Calculated pressure sensitivity as a function of fibre radius. The different curves are for outer jacket layers with different Young's moduli, E_Y. The bulk modulus, K_b, was kept the same (4 GPa) in each case.*

The sensitivity of this fibre was investigated using the plane-strain model. A hydrostatic boundary condition was chosen, this being the most appropriate for a long fibre. An outer jacket, layer four, was included. The radius and Young's modulus of this layer was varied while the bulk modulus, K_b, was fixed at a value of 4 GPa. The set of pressure sensitivity curves that resulted from these calculations are shown in figure 7.

As the coating gets very thick the pressure sensitivity approaches a limit which is independent of the Young's moduli. This suggests that for very thick coatings the magnitude of the strains in the fibre are dependent on the bulk moduli alone. Figure 8 confirms this to be the case. In this calculation the radius of the outer layer was fixed at 3 mm and Young's modulus set at 0.1 GPa. The curve is inversely proportional to the bulk modulus, *i.e.*, linear with the compressibility, of the outer layer. At smaller radii the sensitivity relationship is more complicated, being a function of changes in both elastic moduli.
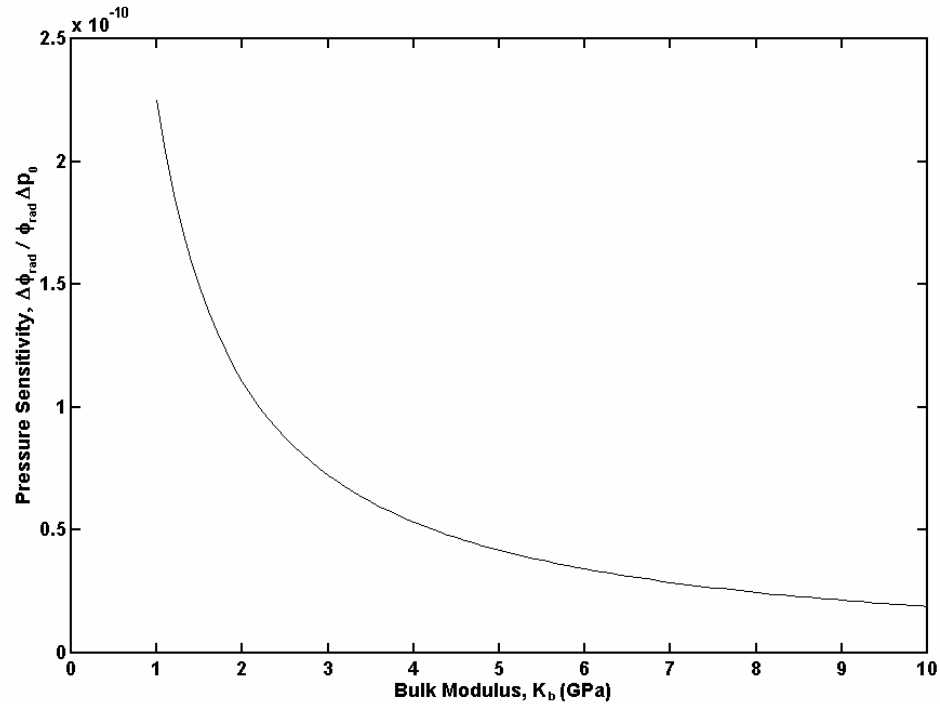
Figure 8 *Calculated pressure sensitivity as a function of bulk modulus, K_b, for a large radius (3 mm) outer jacket. Young's modulus, E_Y, was kept constant (0.1 GPa).*

These results demonstrate that a greatly enhanced pressure sensitivity can be achieved using a clad, rather than an unclad, fibre [32]. This can be further improved by using a coating with a high compressibility, which is precisely the case for non-metallised fibre optic cables. It has been demonstrated that fibres with metal cladding layers are much less sensitive than fibres clad with low bulk modulus materials [33]. Non-metallised submarine telecommunication cables may be particularly suited to detection by this method.

6 OTDR Experiment

The feasibility of using a conventional OTDR to detect acoustically generated stresses in an optic fibre was investigated. The purpose of this investigation was to determine whether an OTDR, of the kind that is commonly used in the telecommunication industry, could be applied directly to the cable detection problem.

The particular device that was used (an Anritsu MW9070A OTDR) exhibited an optical bandwidth of around 60 nm [34]. That is to say, at an optical wavelength of 1 550 nm the optical bandwidth of the OTDR would have been around 5 THz. This is much greater than the Brillouin frequency shift in silica which is ± 11 GHz. Therefore, it should be noted that this device was not capable of isolating Brillouin back-scattered signals from the back-scattered Rayleigh signal since its output would have encompassed all the back-scattered signals that existed within the optical bandwidth.

The apparatus is depicted in figure 9. The OTDR was connected to a 1.8 km length of monomode optic fibre. The properties of this fibre were similar to those of the fibre presented in table 1. The outer jacket was made of acrylic and the overall diameter was around 1 mm. The end of the fibre was clipped to give a strong reflection, which was easy to identify in the OTDR back-scatter trace. The acoustic source was purpose-built using a piezo-ceramic tube transducer encapsulated in a light-duty epoxy resin.
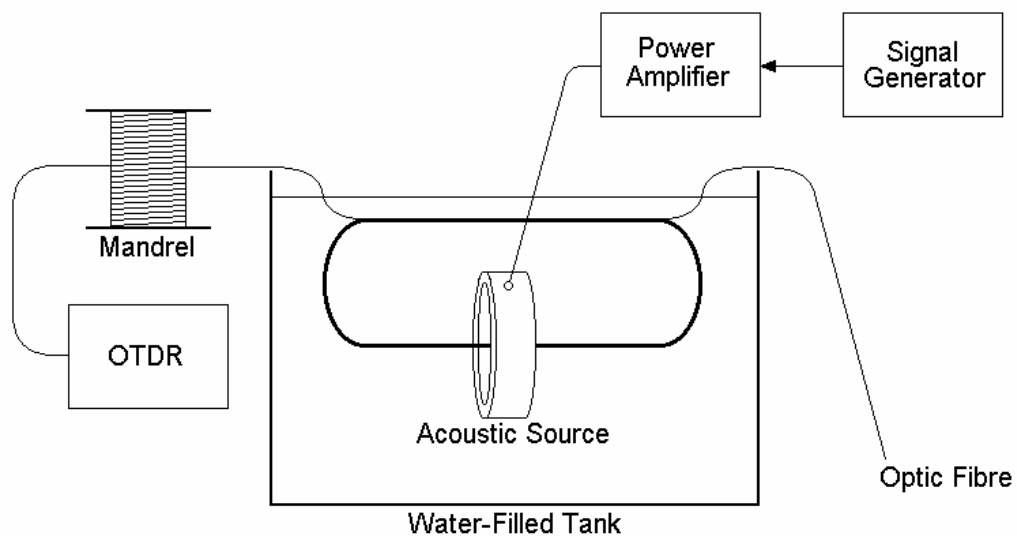
Figure 9 *The apparatus used in the OTDR experiment. The OTDR was connected to a 1.8 km length of optic fibre wound on a mandrel. The final 8 m of fibre was wound through a submerged tubular acoustic source. The fibre was excited using the acoustic source, and the back-scattered optical signal was measured using the OTDR.*

The final 8 m of fibre was wound 10 times through the centre of the tube transducer, with the final metre left to hang freely. Eight frequencies were identified at which the acoustic source was found to be capable of producing an on-axis sound pressure level of 210 dB re 1 μPa. At a wavelength of 1 550 nm, the shortest duration optical pulses that the OTDR could generate were 20 ns. This duration corresponded to a pulse length of 4 m in the fibre. The output trace was adjusted to measure the back-scattered optical power in a 4 m length of fibre ending 1 m before the reflective end.
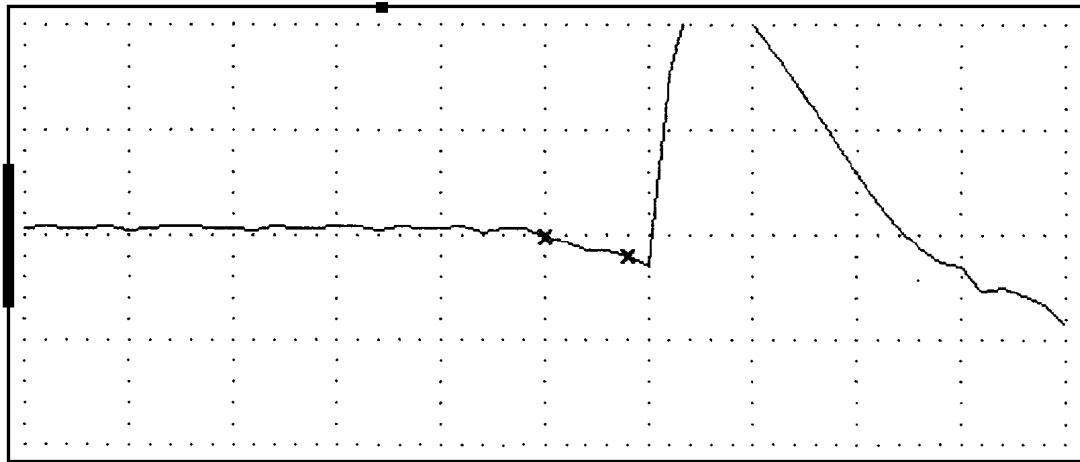
Wavelength: 1 550 nm
Pulse Width: 20 ns
Index of Refraction: 1.466

Horizontal Scale: 0.005 km / division
Vertical Scale: 5.00 dB / division
Cursor Positions: 1.748 km and 1.752 km

Figure 10 An example of the OTDR output trace with no acoustic excitation. Back-scattered optical power is displayed as a function of distance. The decrease in the region between the two cursors was caused by radiation at bends in the fibre. The distinct reflection from the end of the fibre can be seen one metre beyond this region. (Note that the end-reflection has been clipped to allow the region between the two cursors to be resolved.)

This meant that, at the start of the OTDR measurement, the leading edge of the optical pulse would have reached the middle of the length of fibre wound through the

acoustic source. The trailing edge of the pulse would have just entered this region of the fibre. Similarly, at the finish of the OTDR measurement, the leading edge of the pulse would have reached the end of the wound length of the fibre. The trailing edge would have reached the middle of this region of the fibre. Hence, throughout the 4 m OTDR measurement window, the optical pulse would have resided entirely within the region of fibre that could have been excited by the acoustic source.
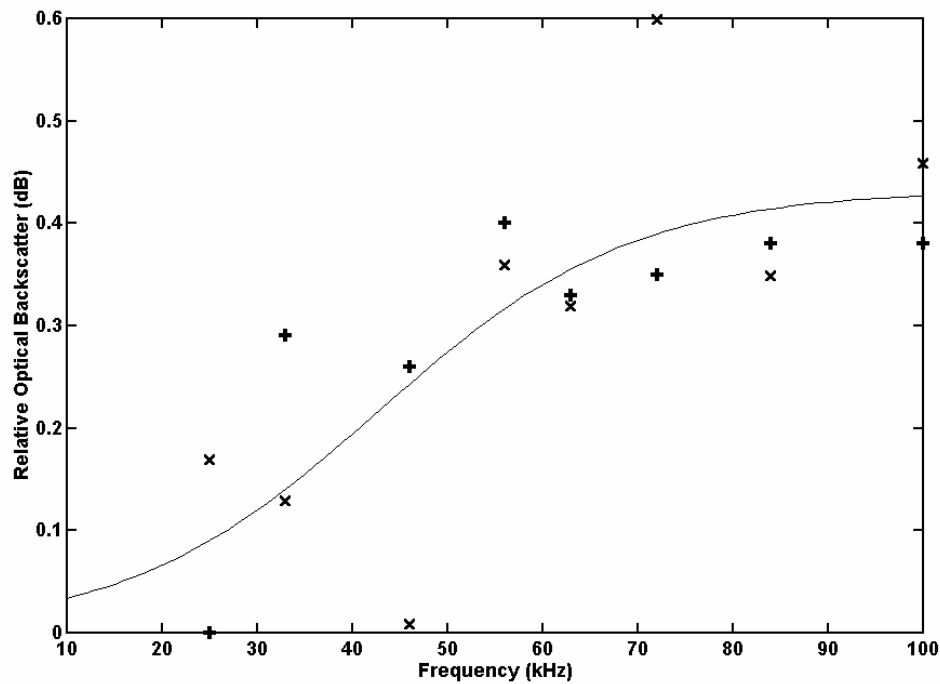
Figure 11 *Two sets of data (+, ×) showing back-scattered optical power in decibels as a function of the acoustic excitation frequency. The values were calculated relative to the back-scattered optical power in the case when there was no acoustic excitation. A best-fit curve for the combined data sets is shown by the solid curve.*

An example of the OTDR output trace is shown in figure 10. In the case shown the fibre was not excited by the acoustic source. The back-scattered power in the measurement region (between the two cursors) reduces at a significantly greater rate than in the fibre before this region. The increase in loss is due to the radiation of

optical power from the bends in the section of fibre wound through the tube transducer.

The back-scattered optical signal was measured with no acoustic excitation and with a 210 dB re 1 µPa excitation at each of the output frequencies. In order to be certain of a statistically significant result, 1 000 averages of the signal were performed in each case. The measurements were then repeated to check that they were consistent.

Under the influence of an acoustic field, the back-scattered optical power was observed to increase over the OTDR measurement window. Changes in back-scatter as a function of acoustic frequency for the two sets of measurements are presented in figure 11. In this instance, 'change' is defined as being the difference, in decibels, between the measurements with and without acoustic excitation. In other words, the figure shows the back-scattered optical power measured in decibels relative to the back-scattered optical power with no acoustic excitation.

It was expected that the coupling between the fibre and the acoustic field would improve as the acoustic wavelength decreased, implying that the back-scattered optical power should increase with frequency. This is consistent with the change that was observed. That is to say, the data points in figure 11 tend, asymptotically, towards a maximum value at high frequencies. A simple model that is consistent with this behaviour is the sigmoid:

$$W_{dB} = \frac{a}{1 + b\exp(-cf_k)} \tag{15}$$

where W_{dB} is the optical back-scatter relative to the case when there was no acoustic excitation, and f_k is the acoustic frequency in kHz. A linear regression was performed for the data presented in the graph, resulting in the following values for the three fitting parameters[11]: a = 0.433 dB; b = 24.8; and c = 0.0753 s. The standard error on the curve model was estimated to be 0.10 dB.

---

[11] Linear regression algorithms attempt to produce models having the least standard error between themselves and the data. They do not automatically produce error estimates. However, examination of a family of fitted curves

A model of this form could be applied to measurements performed on a real telecommunication cable in the future. If combined with the attenuation spectra of the ocean and the seabed, an optimum acoustic operating frequency could be determined in a similar way to the determination of the optimum frequency band (detailed in section 3.2 of the fourth report in this series[4]). It is expected that the optimum frequency would coincide with the geometry of the cable, *i.e.*, $ka_t = 1$. However, this supposition is subject to experimental verification in the marine environment.

This result has confirmed that acoustically generated stresses can cause a change in the back-scattered optical power, as measured using a conventional OTDR. However, the observed change was found to be very small (*i.e.*, the change in optical power was around 0.5 dB for a sound pressure level of 210 dB re 1 µPa).

Therefore, it has been concluded that for a cable detection system of this kind to be successful, a specially designed OTDR would be required (such as an OTDR designed to measure the Brillouin shift, or a sensitive interferometric system designed to measure changes in phase).

7 Summary

An alternative to the remote acoustic approach to the detection of buried objects has been considered for the special case of buried fibre optic communication cables. It was the aim of this report to investigate the theory surrounding such a system, and to assess the feasibility of its practical use.

The use of optic fibres as distributed sensors has been discussed. The most notable example of such a system is the OTDR. Non-linear optical processes that could be exploited in a distributed sensor have also been discussed. The Brillouin effect was given special consideration. It was noted that the associated Brillouin frequency shift depends on variations in temperature and, of particular interest, variations in strain.

The related, acousto-optic effect, was investigated in section 5. It was shown that both length and refractive index changes (in response to an applied strain) can cause a

---

suggests that the stated errors in the parameters a, b and c are, respectively, ± 0.1, ± 5, and ± 0.02. Hence, the 3 significant figures to which the fitted parameters are quoted should be viewed with caution.

change in the optical phase within a fibre. Moreover, pressure sensitivity was shown to be related to the elastic properties of the fibre jacket material. A greatly enhanced sensitivity is predicted if the cladding has a high compressibility (which is expected to be the case for non-metallised fibre optic cables).

An experiment was performed to investigate whether a conventional OTDR could be used to detect acoustically-generated stresses within an optic fibre. A change in the back-scattered power in the optical window of the detector was found to occur. A simple curve model, conforming to the expected behaviour of the system, was subsequently fitted to the experimental data.

In the experiment (detailed in section 6) the change that was observed was very small. It was concluded that an OTDR system, specifically designed to pick out the Brillouin frequency shift, or an interferometric system designed to pick up small changes in optical phase, would be required for the acousto-optic detection approach to work in practice.

The strain dependence of the Brillouin shift (section 4.2) was estimated to be around 130 Hz / kPa. At optical wavelengths of around 1 500 nm in glass, this corresponds to a change in the phase of the Brillouin signal ($\Delta\phi_{rad} / \phi_{rad} \Delta p_0$) of only 10^{-15} Pa^{-1}. For the acousto-optic effect, the change in phase of the optical signal was expected to be significantly larger (see section 5). For a fibre having a relatively thick and compressible cladding, it was calculated to be of the order of 10^{-10} Pa^{-1}.

The sensitivity values for a real fibre optic cable buried in marine sediment are unknown, although they are expected to be similar to the values predicted (above) for the Brillouin and acousto-optic effects. Therefore, it is surmised that an acoustic pressure amplitude in excess of 100 kPa would be required to be incident on the cable to achieve a measurable effect[12], given that a sensitivity of around 1 part in 10^7 can be achieved using interferometric techniques.

This area of study has been taken as far as possible with the laboratory facilities that were made available. However, there are still a number of questions that need to be

---

[12] There exist experimental sources, capable of generating acoustic pressures high enough to remotely detonate underwater mines [35]. However, little has been published regarding their effective range, directivity or frequency response characteristics.

resolved. In particular, the acoustic pressure amplitude required to produce a measurable effect in a cable buried in sand has not been measured. This may form the basis of a future study if the acousto-optic detection technique is ever considered for use in the field.

This material formed the basis of the PhD of RCPE [36-39].

APPENDIX A

OPTIC FIBRE PRESSURE SENSITIVITY

A.1 Calculation of Pressure Sensitivity

The change in relative phase between a light beam entering and leaving an optic fibre provides a measure of the change in pressure experienced by the fibre. Variations in relative phase are observed as modulations in the intensity of light in the interference pattern formed by the incident and transmitted beam.

A jacketed, single mode optic fibre may be represented as a multilayer cylinder as shown in figure A 1. The layers consist of glass of different refractive indices with an outer coating of plastic insulation.
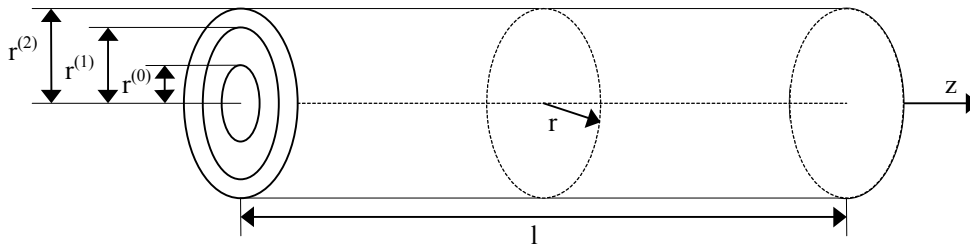
Figure A 1 *The geometry of the multi-layered cylinder representation of a jacketed optic fibre.*

A plane-strain model [30] of the induced phase change for a specific pressure change in a multilayer fibre, assuming that it is subjected to either hydrostatic or radial compression, is presented below. In the radial case, the axial stress at the ends of the fibre is set equal to zero ($\sigma_z = 0$ at $z = 0$ and $z = l$). Let p_0 be the pressure acting on the outer surface of the fibre. In the hydrostatic case, the pressure, p_0, is assumed to be

applied uniformly to the fibre. Therefore, the axial stress at the ends is - p_0. In either case, axial symmetry is assumed.

Polar stresses in the fibre are related to the strains as follows:

$$\begin{bmatrix} \sigma_r^{(i)} \\ \sigma_\theta^{(i)} \\ \sigma_z^{(i)} \end{bmatrix} = \begin{bmatrix} \lambda^{(i)} + 2\mu^{(i)} & \lambda^{(i)} & \lambda^{(i)} \\ \lambda^{(i)} & \lambda^{(i)} + 2\mu^{(i)} & \lambda^{(i)} \\ \lambda^{(i)} & \lambda^{(i)} & \lambda^{(i)} + 2\mu^{(i)} \end{bmatrix} \times \begin{bmatrix} \varepsilon_r^{(i)} \\ \varepsilon_\theta^{(i)} \\ \varepsilon_z^{(i)} \end{bmatrix} \tag{A 1}$$

where the σ terms are stresses, the ε terms are strains and the subscripts, r, θ and z, relate to the radial, torsional and axial components. The index, i, denotes the fibre core layer where i = 0 is the core. The Lamé parameters [20], λ and μ, are related to the Young's modulus, E_Y, and Poisson's ratio, ν, of the fibre by,

$$\lambda^{(i)} = \frac{\nu^{(i)} E_Y^{(i)}}{\left(1 + \nu^{(i)}\right)\left(1 - 2\nu^{(i)}\right)}; \quad \mu^{(i)} = \frac{E_Y^{(i)}}{2\left(1 + \nu^{(i)}\right)} \tag{A 2}$$

For a cylinder, the strains can be obtained from the Lamé solutions,

$$\varepsilon_r^{(i)} = U_0^{(i)} + \frac{U_1^{(i)}}{r^2}; \quad \varepsilon_\theta^{(i)} = U_0^{(i)} - \frac{U_1^{(i)}}{r^2}; \quad \varepsilon_z^{(i)} = W_0^{(i)} \tag{A 3}$$

where $U_0^{(i)}$, $U_1^{(i)}$ and $W_0^{(i)}$ are the parameters that must be determined to find the strains at the radius, r. Since the strains must be finite at the centre of the core, $U_1^{(0)} = 0$. Also, since the axial strain must be, in effect, the same for every layer in the fibre, the parameter, $W_0^{(i)}$, simply becomes W_0.

Expanding equation (A 1) gives

$$\sigma_r^{(i)} = \left(\lambda^{(i)} + 2\mu^{(i)}\right)\varepsilon_r^{(i)} + \lambda^{(i)}\varepsilon_\theta^{(i)} + \lambda^{(i)}\varepsilon_z^{(i)}$$
$$\sigma_\theta^{(i)} = \lambda^{(i)}\varepsilon_r^{(i)} + \left(\lambda^{(i)} + 2\mu^{(i)}\right)\varepsilon_\theta^{(i)} + \lambda^{(i)}\varepsilon_z^{(i)} \tag{A 4}$$
$$\sigma_z^{(i)} = \lambda^{(i)}\varepsilon_r^{(i)} + \lambda^{(i)}\varepsilon_\theta^{(i)} + \left(\lambda^{(i)} + 2\mu^{(i)}\right)\varepsilon_z^{(i)}$$

and substituting the Lamé solutions from equation (A 4),

$$\sigma_r^{(i)} = \left(\lambda^{(i)} + 2\mu^{(i)}\right)\left(U_0^{(i)} + \frac{U_1^{(i)}}{r^2}\right) + \lambda^{(i)}\left(U_0^{(i)} - \frac{U_1^{(i)}}{r^2}\right) + \lambda^{(i)}W_0$$

$$\sigma_\theta^{(i)} = \lambda^{(i)}\left(U_0^{(i)} + \frac{U_1^{(i)}}{r^2}\right) + \left(\lambda^{(i)} + 2\mu^{(i)}\right)\left(U_0^{(i)} - \frac{U_1^{(i)}}{r^2}\right) + \lambda^{(i)}W_0$$

$$\sigma_z^{(i)} = \lambda^{(i)}\left(U_0^{(i)} + \frac{U_1^{(i)}}{r^2}\right) + \lambda^{(i)}\left(U_0^{(i)} - \frac{U_1^{(i)}}{r^2}\right) + \left(\lambda^{(i)} + 2\mu^{(i)}\right)W_0$$

(A 5)

Under the assumption that radial pressure is uniform, there is no torsional stress component so $\sigma_r^{(i)} = \sigma_\theta^{(i)}$. By equivalence of the terms in equation (A 5) and setting $\dfrac{U_1^{(0)}}{r^2} = 0$,

$$\sigma_r^{(i)} = 2\left(\lambda^{(i)} + \mu^{(i)}\right)U_0^{(i)} + \frac{2\mu^{(i)}U_1^{(i)}}{r^2} + \lambda^{(i)}W_0$$

$$\sigma_z^{(i)} = 2\lambda^{(i)}U_0^{(i)} + \left(\lambda^{(i)} + 2\mu^{(i)}\right)W_0$$

(A 6)

The radial ($u^{(i)}$) and axial ($w^{(i)}$) displacements are obtained from the Lamé solutions,

$$u^{(i)} = U_0^{(i)}r + \frac{U_1^{(i)}}{r} \; ; \quad w^{(i)} = W_0 z$$

(A 7)

To solve equation (A 3) it is necessary to establish a set of boundary conditions. For a fibre with n layers, the continuity of stress at each layer boundary is

$$\sigma_r^{(i)}\Big|_{r=r^{(i)}} = \sigma_r^{(i-1)}\Big|_{r=r^{(i)}} \; ; \quad i=1...n-1 \tag{A 8}$$

and the continuity of displacement at each layer boundary is

$$u_r^{(i)}\Big|_{r=r^{(i)}} = u_r^{(i-1)}\Big|_{r=r^{(i)}} \; ; \quad i=1...n-1 \tag{A 9}$$

The radial stress on the outer layer of the fibre is

$$\sigma_r^{(n-1)} = -p_0 \tag{A 10}$$

where p_0 is the pressure acting on the outer surface of the fibre.

An effective axial strain is chosen so that the net axial force, F, satisfies the boundary conditions at the end of the fibre:

$$F = \sum_{i=1}^{n-1} \pi \left(r^{(i)2} - r^{(i-1)2} \right) \left[2\lambda^{(i)} U_0^{(i)} + \left(\lambda^{(i)} + 2\mu^{(i)} \right) W_0 \right]$$
$$+ \pi r^{(0)2} \left[2\lambda^{(0)} U_0^{(0)} + \left(\lambda^{(0)} + 2\mu^{(0)} \right) W_0 \right] \tag{A 11}$$

For the radial model, $F = 0$, and for the hydrostatic model, $F = -\pi p_0 r^{(n-1)2}$.

Applying these conditions to equations (A 6), (A 7), and (A 8) leads to a set of simultaneous equations. The exact number depends on the number of layers in the fibre. The Lamé parameters are found from their solution, and substitution into equation (A 3) gives the strains, ε_r and ε_z, in the core in response to a pressure, p_0, acting on the outer surface of the fibre.

References

[1]   Blomme E, Leroy O, Sliwinski A, "Light Diffraction and Polarization Effects in Isotropic Media with Acoustically Induced Anisotropy", *Acustica*, Volume 82, pp. 464-477, 1996.

[2]   DePaula R P, Flax L, Cole J H, Bucaro J A, "Single-Mode Fiber Ultrasonic Sensor", *IEEE Journal of Quantum Electronics*, Volume QE-18, Number 4, pp. 680 – 683, April 1982.

[3]   Wait P C, *The application of Brillouin scattering to distributed fibre optic sensing*, PhD Thesis, University of Southampton, 1996.

[4]   Hecht E, *Optics*, 2nd Edition, Addison-Wesley Publishing Company, pp. 56 - 68, 1987.

[5]   Hecht E, *Optics*, 2nd Edition, Addison-Wesley Publishing Company, p. 171, 1987.

[6]   Noguchi K, "A 100 km long single-mode optical-fiber fault location", *Journal of Lightwave Technology*, pp. 1 - 6, 1984.

[7]   Wright S, Richards K, Salt S, Wallbank E "High dynamic range coherent reflectometer for fault location in monomode and multimode fibres", *Proceedings of the 9th European Conference on Optical Communication*, pp. 177 - 180, Geneva, 1983.

[8]   Rourke M D, Jensen S M, Barnoski M K, "Fiber parameter studies with the OTDR", Hughes Research Laboratories, Malibu, CA 90265. (Bendow, Mitra, *Fibre Optics*, pp. 255 - 268, Plenum Press, 1978.)

[9]   Conduit A J, *Time-Domain Reflectometry Techniques for Optical Communication*, PhD Thesis, University of Southampton, Department of Electronics, January 1982.

[10]   Dunlop J, Smith D G, *Telecommunications Engineering*, Van Nostrand Reinhold (UK) Co. Ltd., pp. 399 - 400, 1984.

[11]   Marcuse D, "Curvature loss formula for optical fibers", *Journal of the Optical Society of America*, Volume 66, Number 3, pp. 216 - 220, March 1976.

[12]   Takashima S, Kawase M, Tomita S, "Water Sensing Method with OTDR and Optical Sensor for Non-pressurized Optical Fiber Cable System", *IEICE Trans. Commun.*, Volume E77-B, Number 6, pp. 794-799, June 1994.

[13]   Stolen R H, "Nonlinearity in fiber transmission", *Proceedings of the IEEE*, Volume 68, Number 10, pp. 1232 - 1236, October 1980.

[14]   Hecht E, *Optics*, 2nd Edition, Addison-Wesley Publishing Company, pp. 555 - 556, 1987.

[15]   Shen Y R, Bloembergen N, "Theory of stimulated Brillouin and Raman scattering", *Physical Review*, Volume 137, Number 6A, pp. 1787 - 1805, March 1965.

[16]   Hecht E, *Optics*, 2nd Edition, Addison-Wesley Publishing Company, pp. 250 - 252, 1987.

[17]   Arnold J M, "Solitons in Communications", *IEE Electronics & Communication Engineering Journal*, Volume 8, Number 2, pp. 88 - 96, April 1996.

[18]   Hecht E, *Optics*, 2nd Edition, Addison-Wesley Publishing Company, p. 175, 1987.

[19]   Bell J, "Scattered light checks health of optical links", *Opto & Laser Europe*, Issue 44, October 1997.

[20] Timoshenko S, *Theory of Elasticity*, Engineering Societies Monographs, McGraw-Hill Book Company, Inc., New York and London, Chapter 12, 1934.

[21] *Handbook of Chemistry and Physics*, The Chemical Rubber Co., 46th Edition, 1965-1966.

[22] Xu J, Stroud R, *Acousto-Optic Devices: Principles, Design, and Applications*, John Wiley and Sons, Inc., New York, Appendix E, 1992.

[23] Van Vlack L H, *Elements of Materials Science and Engineering*, 6th Edition, Addison-Wesley Publishing Company, pp. 252 - 254, 1989.

[24] Mallinder F P, Proctor B A, *Physics and Chemistry of Glasses*, Volume 5, p. 91, 1964.

[25] Kinsler L E, Frey A R, Coppens A B, Sanders J V, *Fundamentals of Acoustics*, 3rd Edition, John Wiley & Sons, Appendix 10, 1982.

[26] Nash P, "Review of interferometric optical fibre hydrophone technology", *IEE Proceedings, Radar, Sonar and Navigation*, Volume 143, Number 3, pp. 204-209, June 1996.

[27] Hecht E, *Optics*, 2nd Edition, Addison-Wesley Publishing Company, pp. 339 - 361, 1987.

[28] Duncan T, *Physics: A Textbook for Advanced Level Students*, 2nd Edition, John Murray (Publishers) Ltd, p. 423, 1987.

[29] Budiansky B, Drucker D C, Kino G S, Rice J R, "Pressure sensitivity of a clad optical fiber", *Applied Optics*, Volume 18, Number 24, pp. 4085-4088, December 1979.

[30] Hughes R, Jarzynski J, "Static pressure sensitivity amplification in interferometric fiber-optic hydrophones", *Applied Optics*, Volume 19, Number 1, pp. 98-107, January 1980.

[31] Lagakos N, Bucaro J A, Hughes R, "Acoustic sensitivity predictions of single-mode optical fibers using Brillouin scattering", *Applied Optics*, Volume 19, Number 21, pp. 3668-3670, November 1980.

[32] Lagakos N, Schnaus E U, Cole J H, Jarzynski J, Bucaro J A, "Optimizing Fiber Coatings for interferometric Acoustic Sensors", *IEEE Journal of Quantum Electronics*, Volume QE-18, Number 4, pp. 683–689, April 1982.

[33] Lagakos N, Bucaro J A, "Pressure desensitization of optical fibers", *Applied Optics*, Volume 20, Number 15, 2716-2720, August 1981.

[34] *Anritsu MW9070A Optical Time-Domain Reflectometer Operation Manual*, Anritsu Corporation, 5-10-27, Minami-Azabu, Minato-Ku, Tokyo 106.

[35] Mullins J, "Mine smasher", *New Scientist*, p. 11, 18 October 1997.

[36] Evans, R C P, "Acoustic penetration of the seabed, with particular application to the detection of non-metallic buried cables", *PhD Thesis, University of Southampton,* 1999

[37] Evans R C. Leighton T G, "The Detection of cylindrical objects of low acoustic contrast buried in the seabed", *J. Acoust. Soc. Am.*, Vol. 103, p. 2902, 1998.

[38] Evans R C,. Leighton T G, "The Detection of Cylindrical Objects of Low Acoustic Contrast Buried in the Seabed", *Proceedings of the 16th International Congress on Acoustics and 135th Meeting of the Acoustical Society of America (ICA/ASA '98)*, Edited by Kuhl P K and Crum L A, pp. 1369 - 1370, 1998.

[39] Evans R C, Leighton T G, "An experimental investigation of acoustic penetration into sandy sediments at sub-critical grazing angles", *Proceedings of the Fourth European Conference on Underwater Acoustics*, Edited by Alippi A and Cannelli G B, pp. 697 - 702, 1998.